JCTC Journal of Chemical Theory and Computation

pubs.acs.org/JCTC Article

Mechanism of Fully Reversible, pH-Sensitive Inhibition of Human Glutamine Synthetase by Tyrosine Nitration

Benedikt Frieg, Boris Görg, Natalia Qvartskhava, Thomas Jeitner, Nadine Homeyer, Dieter Häussinger,* and Holger Gohlke*

Cite This: *J. Chem. Theory Comput.* 2020, 16, 4694–4705 Read Online

ACCESS | Metrics & More | Article Recommendations | Supporting Information

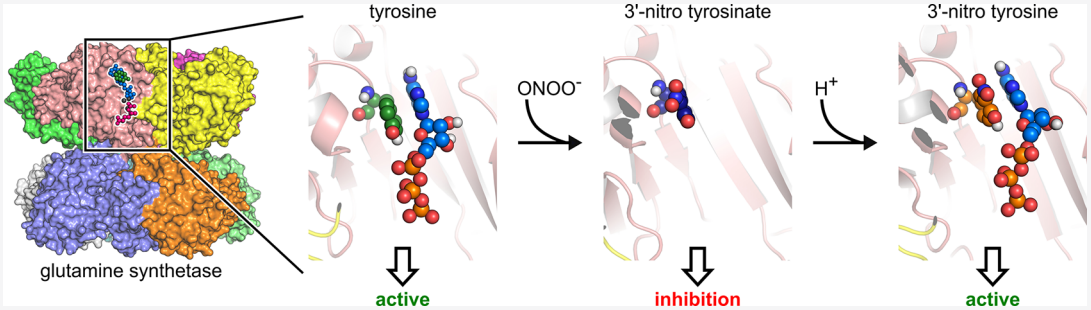

ABSTRACT: Glutamine synthetase (GS) catalyzes an ATP-dependent condensation of glutamate and ammonia to form glutamine. This reaction—and therefore GS—are indispensable for the hepatic nitrogen metabolism. Nitration of tyrosine 336 (Y336) inhibits human GS activity. GS nitration and the consequent loss of GS function are associated with a broad range of neurological diseases. The mechanism by which Y336 nitration inhibits GS, however, is not understood. Here, we show by means of unbiased MD simulations, binding, and configurational free energy computations that Y336 nitration hampers ATP binding but only in the deprotonated and negatively charged state of residue 336. By contrast, for the protonated and neutral state, our computations indicate an increased binding affinity for ATP. pK_a computations of nitrated Y336 within GS predict a pK_a of ∼5.3. Thus, at physiological pH, nitrated Y336 exists almost exclusively in the deprotonated and negatively charged state. *In vitro* experiments confirm these predictions, in that, the catalytic activity of nitrated GS is decreased at pH 7 and 6 but not at pH 4. These results indicate a novel, fully reversible, pH-sensitive mechanism for the regulation of GS activity by tyrosine nitration.

INTRODUCTION

Glutamine synthetase (GS, glutamate ammonia ligase, EC 6.3.1.2) catalyzes the condensation of glutamate and ammonia to form glutamine in a reaction that requires the ATP-dependent phosphorylation of glutamate.[1] Human GS is composed of 10 identical subunits[2] (Figure 1A), with catalytic sites residing in the interfaces of two adjacent subunits. High levels of GS are found in astrocytes,[3] where it is part of glutamate−glutamine cycling,[4] and in perivenous hepatocytes, where it is part of the intercellular glutamine cycle and essential for hepatic ammonia detoxification.[5−7] Ammonia detoxification and glutamine synthesis make GS essential for the human nitrogen metabolism.[8,9] Significant changes in GS activity occur in neurological disorders such as Alzheimer's disease,[10,11] hepatic encephalopathy,[12−14] and epilepsy.[15,16] Thus, elucidating the mechanisms by which GS acts or is regulated will add in the development of new treatment strategies for the aforementioned disorders. Recently, we showed that mutations that cause human GS inhibition and lead to clinically relevant pathologies act to hamper ATP and glutamate binding, the first steps[17] of glutamine formation.[18]

Nitration of tyrosine 336 (Y336; native amino acids are reported according to crystal structure numbering[2] hereafter)[20−24] inhibits human GS activity. This protein tyrosine nitration (PTN) yields 3′-nitro tyrosine[19,25] (in the following named TYN and referring to the nitrated amino acid in solution; Figure 1B) and decreases the pK_a of the phenolic hydroxyl group by three log units.[26] Thus, at physiological pH, nitrated tyrosine exists partially in the deprotonated phenolate form (in the following named TYD and referring to the nitrated, deprotonated amino acid in solution; Figure 1B). PTN is an established biomarker of cellular "nitrooxidative stress".[19]

The structure of human GS complexed with ADP[2] indicates that Y336 forms face-to-face stacking interactions with this

Received: March 14, 2020
Published: June 17, 2020

https://dx.doi.org/10.1021/acs.jctc.0c00249
J. Chem. Theory Comput. 2020, 16, 4694–4705

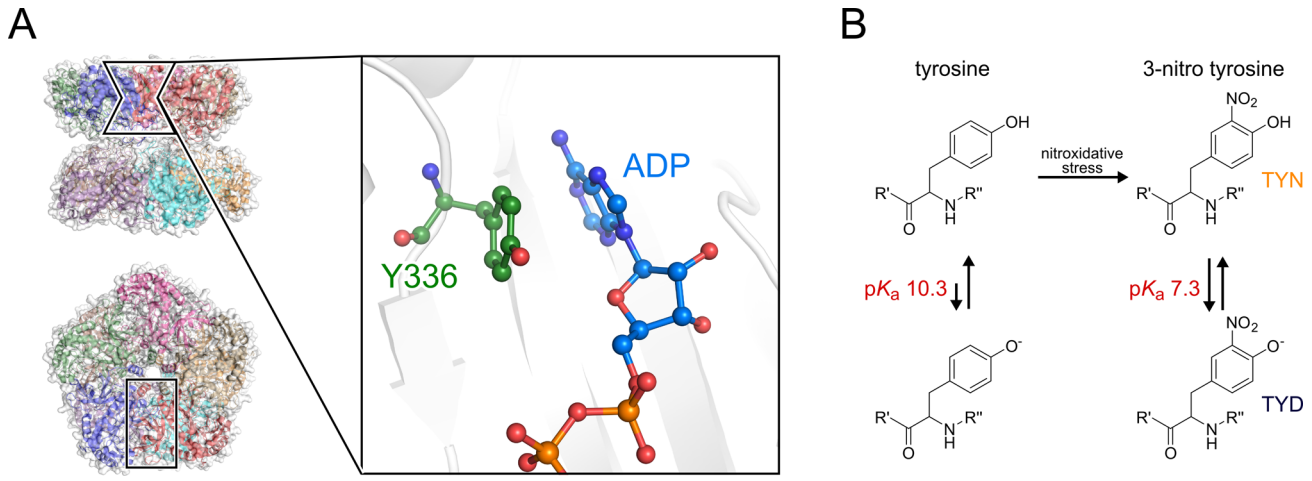

Figure 1. Nitration of Y336 in human GS. (A) Crystal structure of human GS (PDB entry: 2QC8[2]) in side (top) and top view (bottom) and close-up view of the ATP/ADP binding site (right). Each subunit is colored differently and depicted in cartoon-surface representation. Bifunnel[17] and box depict the location of the catalytic site in the GS decamer. ADP (blue) and Y336 (green) are depicted as ball−stick models. (B) Scheme of tyrosine nitration. Nitration causes a decrease in the pK_a of the phenolic hydroxyl group by three log units.[19] At physiological pH (~7.4), both 3′-nitrotyrosine variants TYN and TYD are almost equally populated (panel B is adapted from ref 19). TYN and TYD refers to the nitrated amino acids in solution.

nucleotide (Figure 1A). ADP is formed within the enzyme following phosphorylation of glutamate by ATP. Although no crystal structure of human GS with bound ATP is yet available, Y336 most likely forms similar face-to-face stacking interactions with ATP, which binds to the homologous hydrophobic pocket in the crystal structure of GS from *Helicobacter pylori*.[27] The GS catalytic site is typically depicted as two opposing funnels, conjoined at their apexes, with ATP binding the upper funnel and glutamate binding the lower funnel.[17] Y336 is situated in the upper funnel close to the bound ATP. Substrates other than ATP are ~10 Å away from Y336.[2] An influence of Y336 nitration on other substrates is therefore unlikely. Even so, the mechanism by which Y336 nitration inhibits GS activity at an atomistic level remained elusive.

Here, we investigated the molecular mechanism of how Y336 nitration inhibits human GS activity by a combined computational and experimental study. These investigations included unbiased molecular dynamics (MD) simulations, binding free energy calculations, and potential of mean force (PMF; configurational free energy) computations of the interactions of nitrated Y336 with GS-bound ATP and ATP binding process. *In vitro* activity measurements of GS confirmed the pH sensitivity of nitrated GS, in that, the catalytic activity of nitrated GS is decreased at neutral pH, but not at pH 4. The pH sensitivity of tyrosine-nitrated GS indicates a novel regulation of protein function due to PTN.

MATERIALS AND METHODS

Please see the Supporting Information for a detailed description.

Unbiased Molecular Dynamics Simulations. We performed unbiased MD simulations of wild type GS, GS_{TYN}, and GS_{TYD} bound to ATP with water represented explicitly. The general simulation protocol was adapted from ref 18. After energy minimization, thermalization, and density adaptation, the systems were subjected to 5 × 500 ns of unbiased MD simulations. The MD trajectories were analyzed toward structural features that characterize stacking interactions between ATP and residue Y336/TYN336/TYD336. All simulations were performed using GPU acceleration with the *pmemd.cuda* module implemented in Amber.[28]

Computation of Effective Binding Energies. Subsequent to the MD simulations, we computed effective binding energies. The effective binding energies ($\Delta G_{effective}$) were averaged over five trajectories ($\overline{\Delta G}_{effective}$). Relative effective binding energies ($\Delta\Delta G_{effective}$) were calculated by subtracting the mean $\Delta G_{effective}$ of the wild type ($\overline{\Delta G}_{wild\ type}$) from the effective binding energy of the nitro variant ($\overline{\Delta G}_{nitro}$) (eq 1, Supporting Information). The results are expressed as $\Delta\Delta G_{effective} \pm SEM_{total}$ (eqs 2 and 3, Supporting Information).

Thermodynamic Integration Simulations. Relative binding energies ($\Delta\Delta G_{bind.}$) were calculated by following the TIES protocol[29] (Thermodynamic Integration with Enhanced Sampling). Therefore, the average $\Delta V/\Delta\lambda$ values are calculated as an "ensemble average approach", referring to performing an ensemble of independent simulations to calculate averaged free energies.[29−31] In general, we performed three replica simulations at 13 distinct λ steps (λ = 0.0, 0.05, 0.1, 0.2, ..., 0.9, 0.95, 1.00), applying the one-step softcore approach.[32,33] Technically, we simulated the transformation of TYN336 into Y336 and TYN336 into TYD336 in the GS_{APO} and GS_{ATP} states.

Potential of Mean Force Calculations. We performed PMF (configurational free energy) calculations of ATP unbinding from its binding site within wild type GS, GS_{TYN}, and GS_{TYD}. We computed the PMF of ATP unbinding employing umbrella sampling[34] and the Weighted Histogram Analysis Method (WHAM).[35] As a reaction coordinate d, we used the distance between the centers of mass of Y336/TYN336/TYD336's benzene ring and ATP's purine ring. The resulting PMFs were normalized relative to the completely unbound state.

Calculating pK_a Shifts from Free Energies. To calculate the pK_a shift of TYN336 due to the protein environment, we applied the method reported by Simonson et al.[36] We used TI to calculate ΔG for the transformation of TYN into TYD in our model and TYN336 into TYD336 in the protein structure. In general, we performed three replica simulations at 13

https://dx.doi.org/10.1021/acs.jctc.0c00249
J. Chem. Theory Comput. 2020, 16, 4694−4705

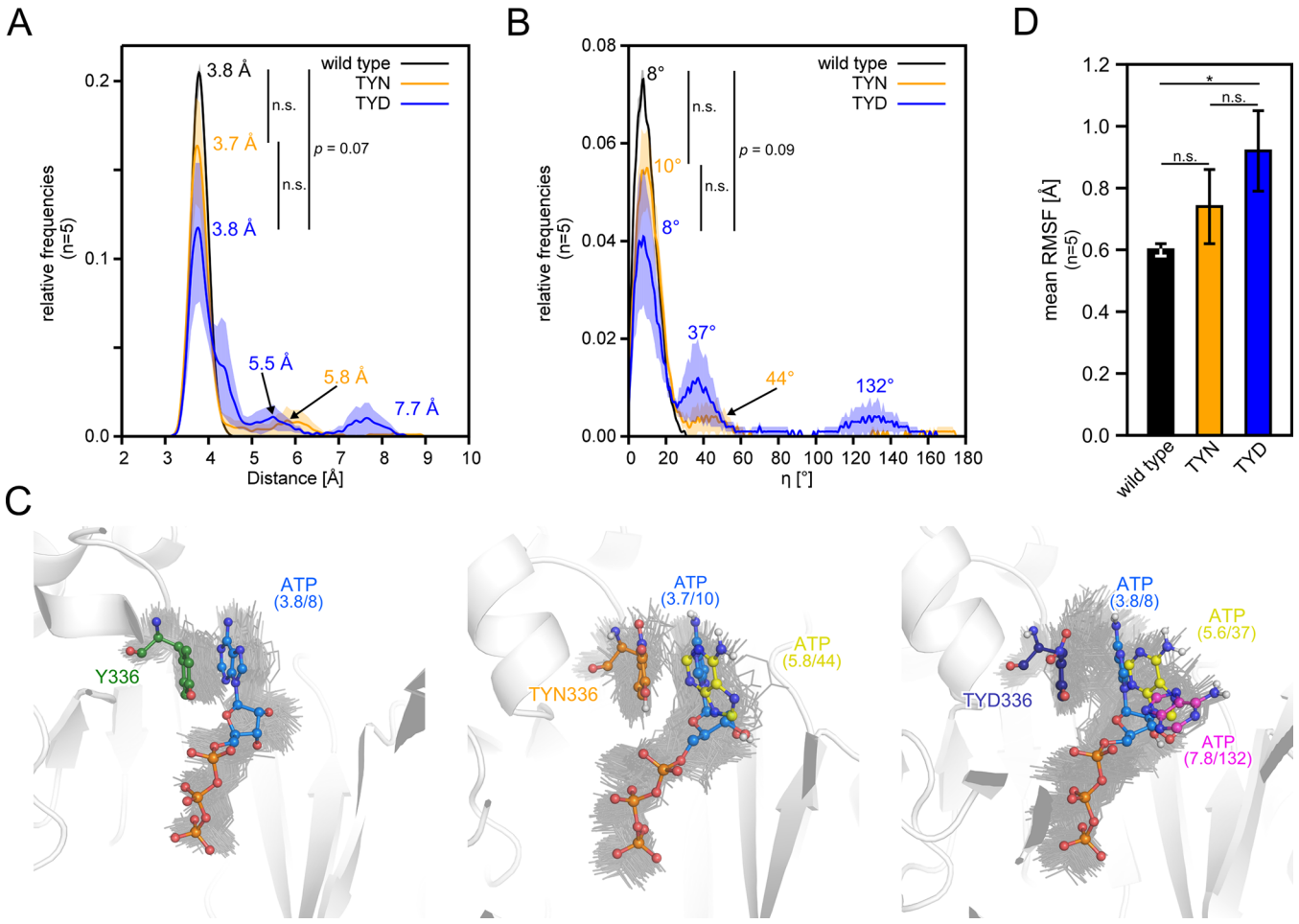

Figure 2. Results from unbiased MD simulations. (A, B) Mean fractional populations (normalized by the sum of all bins) with standard error of the mean (SEM; depicted as filled curve) for (A) the distance between the centers of mass of the phenyl ring (residue Y336 and nitro variants) and the purine ring system (ATP) (bin size 0.1 Å) and (B) the angle between the ring planes of the phenyl ring (residue Y336/TYN336/TYD336) and the purine ring system (ATP) (bin size 1°). (C) Representative structures extracted from the MD trajectory for wild type GS (left), GS_{TYN} (middle), and GS_{TYD} (right). In the foreground, representative ATP configurations belonging to the main populations in panels A and B (see respective labels depicting "distance [Å]/η [°]" combinations) are depicted as opaque ball–stick models. For representative purposes, for ATP molecules that do not belong to the major population, only the adenine system is shown. In the background, an overlay of ATP configurations extracted in 10 ns intervals is depicted as gray sticks that visualize the motion of ATP over the course of the MD simulations. (D) Mean root-mean-square fluctuation (RMSF) with SEM (error bars) calculated for all nonhydrogen atoms in ATP. ∗: Statistically significantly different compared to wild type GS (p <0.05). n.s.: Not significantly different.

distinct λ steps (λ = 0.0, 0.05, 0.1, 0.2, ..., 0.9, 0.95, 1.00), applying the one-step softcore approach.[32,33]

Expression and Purification of Human GS. A plasmid expressing human GS was donated to us by Dr. Norma Allewell and used to transform *E. coli* and to express the enzyme in these cells, as described by Listrom et al.[37] The subsequent purification of human GS was adapted from the methods published by Listrom et al.[37] In brief, clarified sonicates of *E. coli* suspensions expressing human GS underwent successive purification on HA Ultrogel, DEAE–Sepharose, and MonoQ resins, using linear (100–500 mM potassium phosphate buffer (pH 7.2)), step (imidazole–NaOH buffer at pH 7.99), and linear (0–250 mM NaCl in 20 mM Tris-HCl) gradients, respectively. The potassium phosphate buffer also contained 5 mM 2-mercaptoethanol. Similarly, the imidazol–NaOH buffer also contained 1 mM EDTA and 5 mM 2-mercaptoethanol. The first two separations were performed at room temperature, while the final chromatography was carried out at 4 °C and yielded a protein that was greater than 99% pure as judged by SDS-PAGE. The purified human GS was combined with glycerol at a final concentration of 10% and stored at 4 °C. GS activity during the purification was assessed using a hydroxamate assay, as described by Jeitner and Cooper.[38]

Peroxynitrite Treatment of Human GS. Purified human GS was incubated in 0.1 M KH_2PO_4 (pH 7.0) and nitrated by addition of peroxynitrite ($ONOO^-$, in 0.1 M KOH) under constant stirring as described before.[21]

Western Blot Analysis. Western Blot analysis was performed as described before.[21] Briefly, equal amounts of isolated human GS were subjected to sodium dodecyl sulfate polyacrylamid gel electrophoresis (SDS-PAGE) using 10% gels. Blots were probed for 2 h at room temperature with antibodies against 3′-nitrotyrosine (mAb, Upstate) or GS (mAb, Becton Dickinson, 1:5000).

GS Activity Assay. Human GS activity was measured according to ref 39 by using a commercial kit (SPGLUT11, Sigma, Deisenhofen, Germany). In this assay, the conversion of

https://dx.doi.org/10.1021/acs.jctc.0c00249
J. Chem. Theory Comput. 2020, 16, 4694–4705

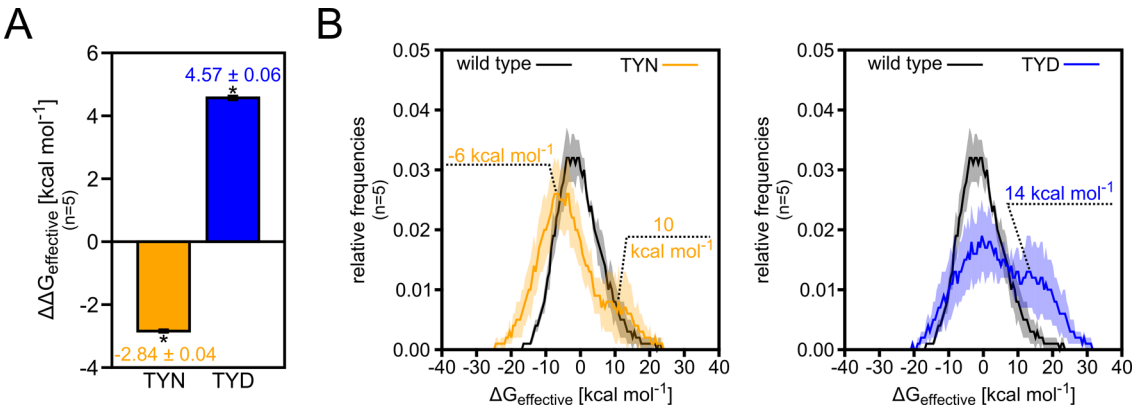

Figure 3. Results from MM-PBSA calculations. (A) Mean relative effective binding energies with respect to wild type GS ($\Delta\Delta G_{effective}$). $\Delta\Delta G$ values were calculated by the MM-PBSA approach for ATP binding to both nitro variants GS_{TYN} (orange) and GS_{TYD} (blue). Error bars indicate SEM_{total} (eq 3, Supporting Information); asterisks indicate a significant difference ($p < 0.05$) between wild type GS and GS_{TYN} or GS_{TYD}, respectively. Labels depict $\Delta\Delta G_{effective} \pm SEM_{total}$ in kcal mol^{-1}. (B) Mean relative frequencies (normalized by the sum of all bins; bin size 0.5 kcal mol^{-1}) of relative effective binding energies and standard error of the mean (filled curve). Effective binding energies of ATP binding to GS_{TYN} (left) or GS_{TYD} (right) were normalized to the mean effective binding energy of ATP binding to wild type GS, such that the histogram for wild type GS was shifted to zero and the GS_{TYN} and GS_{TYD} ones were shifted accordingly.

ATP to ADP by GS is coupled to the oxidation of NADH to NAD^+ by L-lactic dehydrogenase. GS activity in $ONOO^-$-exposed samples is expressed relative to vehicle-treated control at pH 7.0.

RESULTS

Y336 Nitration Weakens Interactions with ATP in the GSTYD Variant. In order to address, at an atomistic level, how Y336 nitration inhibits GS activity, we performed unbiased MD simulations of three GS variants: wild type GS, GS bearing the protonated TYN336 (i.e., GS_{TYN}), and GS bearing the deprotonated TYD336 (i.e., GS_{TYD}), each bound to ATP. For each system, five replicates of MD simulations of 500 ns length each were performed. To characterize the stacking interactions between the phenyl ring of Y336/TYN336/TYD336 and the purine ring system of ATP, we analyzed the MD trajectories with respect to the distance between the centers of mass (COM) and the angle between the planes of these ring systems. The distance measurements indicate that the major populations are found at short distances ($d \approx 3.8$ Å) for all GS variants, although the rank order of these changes decreases from wild type GS to GS_{TYN} to GS_{TYD} (Figure 2A). For both tyrosine-nitrated variants, we found additional populations at longer distances ($d \approx 5.5$ Å) and, exclusively for GS_{TYD}, another one at $d \approx 7.7$ Å (Figure 2A). The shapes of the histograms for the plane angle are similar, with the major population found for an almost parallel orientation of the ring systems ($\eta \approx 8°$) for all GS variants (Figure 2B). Additional populations are found at increased η for GS_{TYN} and GS_{TYD} ($\eta \approx 40°$) and for GS_{TYD} exclusively ($\eta \approx 132°$) (Figure 2B). Finally, we plotted the distances vs η in a 2D histogram (Figure S1). As to wild type GS, the 2D histogram revealed one primary orientation of ATP relative to Y336, in which both are oriented almost in parallel at small distances (Figure S1). The likelihood of this orientation is reduced in GS_{TYN} and, in particular, in GS_{TYD}. These results suggest that Y336 nitration weakens the tyrosine/adenine interaction, especially in the GS_{TYD} variant.

Representative sets of configurations of Y336/TYN336/TYD336 and ATP extracted from the MD trajectories (grayish structures in Figure 2C) indicate that ATP is more mobile after Y336 nitration, in particular, in the region of the adenine moiety. In the wild type, the adenine moiety is stably bound to a predominantly hydrophobic pocket formed by W130, F131, P208, F256, and Y336 (Figure S2). ATP and Y336 are oriented almost in parallel, but as pointed out above, although similar poses were found in GS_{TYN} and GS_{TYD}, their occurrence frequency is lower after nitration (Figures S1 and S2). For both nitrated variants in turn, additional ATP poses are observed, in which the adenine moiety is no longer oriented in parallel to the tyrosine ring (Figure 2C). In the case of GS_{TYD}, we also found conformations, in which TYD336 is no longer involved in adenine binding (magenta conformation in Figure 2C, Figure S2). The adenine moiety has moved to another pocket instead, in which it is partially stabilized by interactions with W60, A191, and P208 (Figure S2). This is likely the consequence of the negatively charged side chain in TYD336, which obviously weakens the hydrophobic stacking interactions with the electron-rich purine system. This finding is confirmed by computing root-mean-square fluctuations (RMSF), a measure for mobility, for all nonhydrogen atoms in ATP after superimposing all GS_{core} (see Supporting Information for details) backbone atoms to the crystal structure. ATP bound to GS_{TYD} shows a significantly increased mobility (RMSF = 0.92 Å ± 0.13 Å; $p < 0.05$) with respect to ATP bound to wild type GS (Figure 2D). By contrast, the mean RMSF between ATP bound to GS_{TYN} or wild type GS ($p = 0.31$), or between ATP bound to GS_{TYN} or GS_{TYD} ($p = 0.34$), do not differ significantly (Figure 2D). These results further support the conclusion that TYD336/ATP interactions are weakened in the GS_{TYD} variant compared to wild type GS.

Y336 Nitration Decreases the Effective Binding Energy of ATP in the GSTYD variant. In order to determine energetic consequences of the Y336 nitration on ATP binding, the effective energies of ATP binding relative to wild type GS ($\Delta\Delta G_{effective}$, eq 1, Supporting Information) were computed using the MM-PBSA approach. The computed $\Delta\Delta G_{effective}$ values indicate that ATP binding is disfavored in GS_{TYD} ($\Delta\Delta G_{effective}$ = 4.57 kcal mol^{-1} ± 0.06 kcal mol^{-1}; $p < 0.01$) but favored in GS_{TYN} ($\Delta\Delta G_{effective}$ = −2.84 kcal mol^{-1} ± 0.04 kcal mol^{-1}; $p < 0.01$) (Figure 3A). The MM-PBSA results for GS_{TYD} are thus consistent with the results of

https://dx.doi.org/10.1021/acs.jctc.0c00249
J. Chem. Theory Comput. 2020, 16, 4694−4705

A

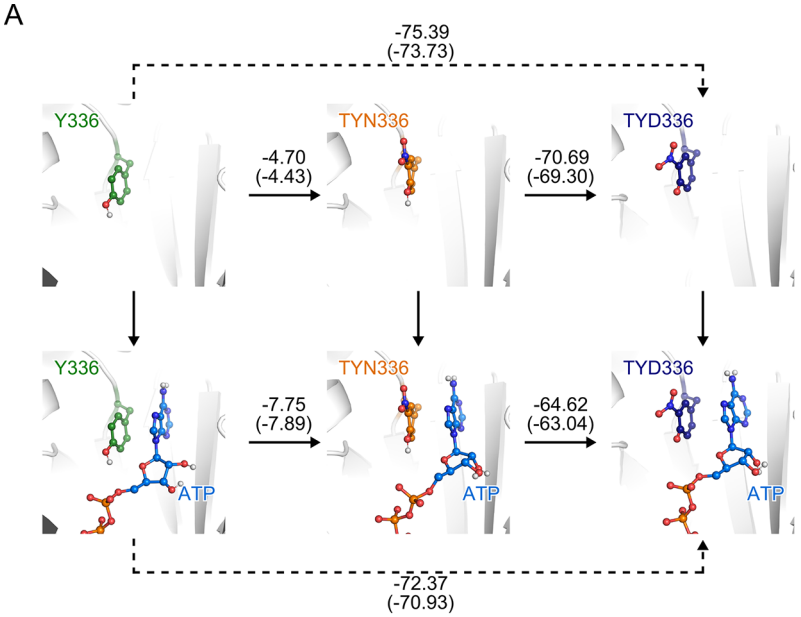

B

$\Delta\Delta G_{bind.}$	Y336 ⟶ TYN336	TYN336 ⟶ TYD336	Y336 ⟶ TYD336
From λ = 0.0 to λ = 1.0	-3.05	6.07	3.02
(Excl. λ = 0.0 and λ = 1.0)	(-3.46)	(6.26)	(2.80)

Figure 4. Relative binding free energies estimated by thermodynamic integration.(A) Thermodynamic cycle to estimate relative binding free energies. The vertical arrows depict the ATP binding process. The horizontal arrows depict the transformation reaction of TYN336 either into Y336 (left cycle) or TYD336 (right cycle). The transformation depicted by the dashed arrow connecting Y336 and TYD336 was not simulated but estimated by employing the principles of the thermodynamic cycle (the sum of the transformations of Y336 into TYN366 into TYD336). The labels above the arrows denote ΔG values derived by integration of the $\Delta V/\Delta\lambda$ curves in Figure S3A–D. If ΔG is reported in parentheses, the endpoints λ = 0.0 and λ = 1.0 were not considered for integration. In the case of the transformation of TYN336 into TYD336, λ = 0.9 was neglected, too. (B) Relative binding free energies ($\Delta\Delta G_{bind.}$) calculated according to eq 4, Supporting Information. Negative (positive) values indicate an energetically favored (disfavored) ATP binding process. All energies are reported in kcal mol^{-1}.

the structural analyses (Figure 2, Figure S2). Analysis of the frequencies of the normalized $\Delta G_{effective}$ computed for configurations along the MD trajectories reveals two main populations for the GS_{TYD} system: one with a maximum at $\Delta G_{effective} \approx 0$ kcal mol^{-1}, which relates to configurations of the major population in Figure 2A, B (distance/η combination: 3.8 Å/8°), and another with a maximum at $\Delta G_{effective} \approx 14$ kcal mol^{-1} (Figure 3B), which relates to configurations that are part of the minor populations in Figure 2A, B (distance/η combinations: 5.5 Å /37° and 7.7/132°). As to GS_{TYN}, the frequencies of normalized $\Delta G_{effective}$ computed for configurations along the MD trajectories also reveal two main populations: one with a maximum at $\Delta G_{effective} \approx -6$ kcal mol^{-1} (Figure 2B), which relates to configurations of the major population in Figure 2A, B (distance/η combination: 3.7 Å/10°) and another that forms a shoulder at $\Delta G_{effective} \approx 10$ kcal mol^{-1}, which relates to configurations of the minor populations in Figure 2A, B (distance/η combination: 5.8 Å/44°). Hence, in both cases, a coplanar arrangement between TYN336 or TYD336 and ATP's purine ring system is energetically neutral or favorable as compared to non-nitrated Y336. Deviations from a coplanar arrangement, as they occur for TYN336 or TYD336 (Figure 2, Figure S2), are energetically disfavorable, mirroring results from *ab initio* calculations.[40] While the results suggest that ATP binding is energetically disfavored in the case of TYD336, providing a plausible explanation for a loss of GS activity upon Y336 nitration,[20−24] the results also suggest that ATP binding is favored in the presence of TYN336, which is controversial to previous experimental studies.[20−24]

To validate the results from MM-PBSA calculations, we performed thermodynamic integration (TI) simulations to derive relative binding free energies for ATP binding. We simulated the transformation of TYN336 into Y336 and TYN336 into TYD336, in both states GS_{Apo} and GS_{ATP}. The $\Delta V/\Delta\lambda$ curves for all transformations are shown in Figure S3A–D, and ΔG values obtained by integration of the $\Delta V/\Delta\lambda$ curves are summarized in Table S1. The thermodynamic cycles for computing relative binding free energies of ATP binding ($\Delta\Delta G_{bind.}$) are shown in Figure 4A. The computed $\Delta\Delta G_{bind.}$ values indicate that ATP binding is disfavored in GS_{TYD} ($\Delta\Delta G_{bind.}$ = 3.02 kcal mol^{-1}; SEM < 0.01 kcal mol^{-1}) but favored in GS_{TYN} ($\Delta\Delta G_{bind.}$ = −3.05 kcal mol^{-1}; SEM < 0.01 kcal mol^{-1}) with respect to wild type GS (Figure 4B). Taken together, the TI results are consistent with the results from MM-PBSA computations (Figure 3), such that two independent methods suggest that Y336 nitration in human GS leads to a decrease in ATP binding relative to wild type GS, but only in the deprotonated and negatively charged TYD336 state. To independently validate the energetic analysis and to further elucidate the effect of Y336 nitration on ATP binding, we next performed PMF computations of ATP binding to GS. PMF computations will provide an energetic estimate of the association/dissociation process of ATP binding, which might also be influenced by TYN336.

https://dx.doi.org/10.1021/acs.jctc.0c00249
J. Chem. Theory Comput. 2020, 16, 4694−4705

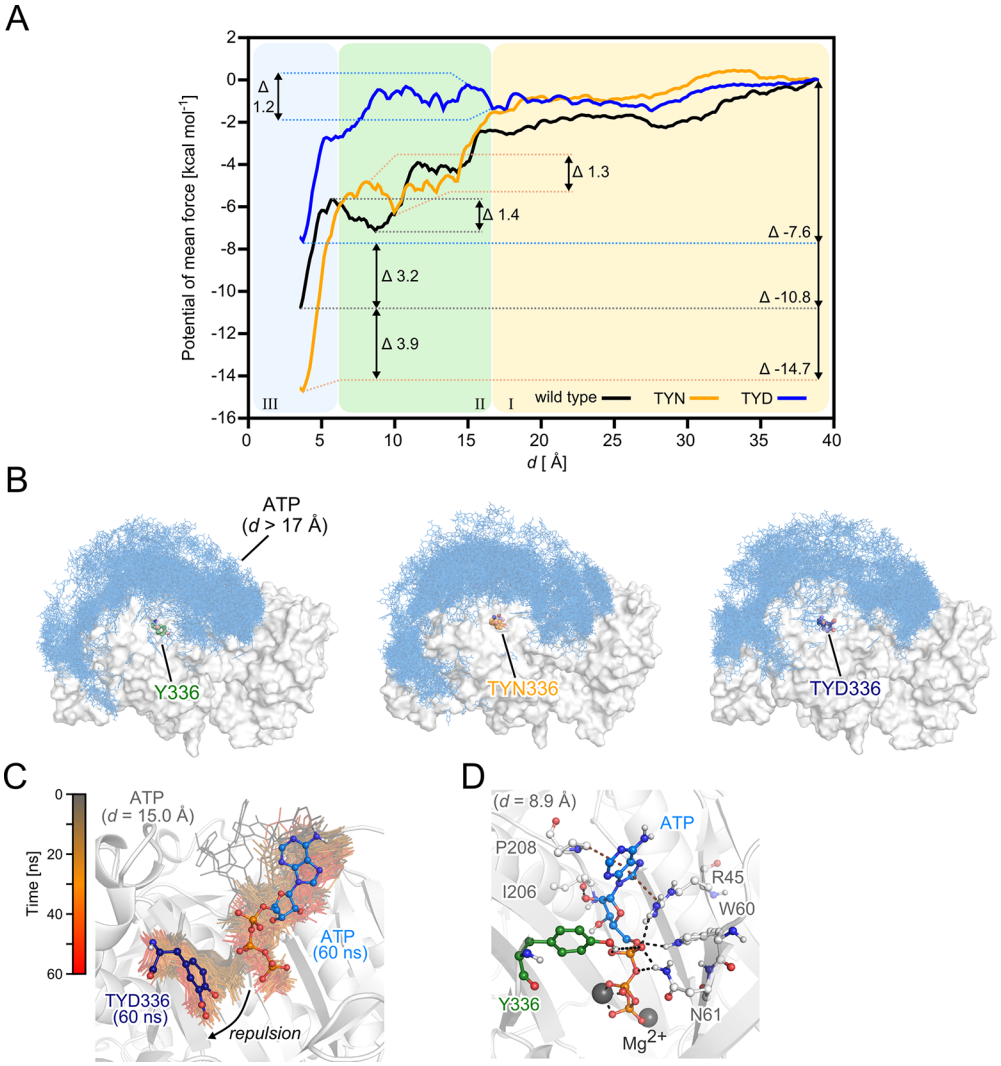

Figure 5. Energetic and structural description of the ATP binding process. (A) Potential of mean force (PMF), derived by umbrella sampling and WHAM, for ATP binding to wild type GS (black), GS_{TYN} (orange), and GS_{TYD} (blue). I (yellow background), II (green background), and III (cyan background) depict the phases of ATP binding. Configurational free energies are normalized relative to the unbound state (d = 38.9 Å). Labels depict relevant changes in the PMF (in kcal mol^{-1}). (B) ATP diffusion for simulations restrained to 17 Å < d < 38.7 Å. ATP poses were extracted in 0.5 ns intervals for wild type GS (left), GS_{TYN} (middle), and GS_{TYD} (right). (C) Time traces of ATP and TYD336 during umbrella sampling simulations (colored according to the color ranges on the left) that were restrained to d = 15.0 Å. An arrow depicts the major motion of TYD336. (D) ATP temporarily bound (at d = 8.9 Å) to wild type GS. The interacting residues of wild type GS are shown as white ball−stick models. Hydrogen bonds are shown as black lines and contacts with purine in ATP as brown lines. In the interest of clarity, in panel B, only the protein starting structures for all variants (white surface) and purine fragments of ATP are shown. All configurations shown were extracted after superimposing the protein structure to the initial structure.

Y336 Nitration Weakly Influences ATP Binding Kinetics. In addition to influencing the thermodynamics of ATP binding, nitration of Y336 might also introduce a steric and/or electrostatic barrier that hampers access of ATP to the binding site and thereby influence the binding kinetics. Hence, to further elucidate the effect of Y336 nitration on ATP binding, we computed the PMFs of ATP binding to the GS variants along a binding path (Figure S4A) determined by random acceleration (expulsion) MD.[41] In agreement with the suggested mechanism of glutamine synthesis by GS, ATP enters and exits the active site via the upper funnel.[17] The triphosphate moiety of ATP is thought first to enter the site and to pass by Y336, along with the ribose unit, to finally position the adenine group close to this residue. Umbrella sampling[34] simulations of this path were performed for wild type GS, GS_{TYN}, and GS_{TYD}, using as a reaction coordinate the distance d between the centers of mass of the phenyl ring of Y336/TYN336/TYD336 and ATP's purine ring system (Figure S4A, B). As the binding path is almost straight, d increases monotonously if ATP unbinds. The PMF was then derived by the Weighted Histogram Analysis Method (WHAM).[35]

The PMFs for all GS variants are consistent with the ATP bound state being markedly favored over the unbound state ($\Delta G_{wild\ type}$ = −10.8 kcal mol^{-1}, $\Delta G_{total,\ TYN}$ = −14.7 kcal mol^{-1}, $\Delta G_{total,\ TYD}$ = −7.6 kcal mol^{-1}; SEM always <0.06 kcal mol^{-1}) (Figure 5A). Relative changes between wild type GS and the 3′-nitro variants ($\Delta\Delta G_{TYD\text{-}wild\ type}$ = 3.34 kcal mol^{-1} and $\Delta\Delta G_{TYN\text{-}wild\ type}$ = −3.9 kcal mol^{-1}) are in good agreement with $\Delta\Delta G$ values from MM-PBSA and TI calculations (Figures 3 and 4). Hence, three independent but related methods

https://dx.doi.org/10.1021/acs.jctc.0c00249
J. Chem. Theory Comput. 2020, 16, 4694−4705

indicate that ATP binding is thermodynamically disfavored in GS_{TYD} but favored in GS_{TYN}.

By contrast, the PMFs suggest that Y336 nitration only weakly influences the kinetics of ATP binding. Going from the unbound state ($d \approx 38$ Å) to the bound state ($d \approx 4$ Å), ATP binding to GS can be separated into three phases (I, II, and III) (Figure 5A). Phase I contains all ATP states with $d > 17$ Å. In this phase, ATP diffuses almost freely on the outside of the protein (Figure 5B), which is reflected in rather flat PMF parts that differ by less than 2.5 kcal mol^{-1} with respect to the reference point at $d = 38.9$ Å. The region explored by ATP during the umbrella sampling simulations is qualitatively the same for all GS variants, such that one can assume that the rotational and translational volume sampled by unbound ATP is also similar in all three cases; hence, from a thermodynamic point of view, the unbound state is equally favorable (or disfavorable) for all GS variants. During phase II of ATP binding (6 Å $< d \leq$ 17 Å), the PMFs reveal similar, small energetic barriers for GS_{TYD} ($\Delta G_{16.7\text{ Å} \rightarrow 14.9\text{ Å}} = 1.2$ kcal mol^{-1}), GS_{TYN} ($\Delta G_{10\text{ Å} \rightarrow 8\text{ Å}} = 1.2$ kcal mol^{-1}), and wild type GS ($\Delta G_{8.7\text{ Å} \rightarrow 6\text{ Å}} = 1.4$ kcal mol^{-1}) (Figure 5A). In the case of GS_{TYD}, the PMF increases ($\Delta G_{16.7\text{ Å} \rightarrow 14.9\text{ Å}} = 1.2$ kcal mol^{-1}) as the ATP's negatively charged phosphate chain passes by the negatively charged TYD leading to repulsion between these moieties (Figure 5C). By contrast, ATP hydrogen bonds with the phenolic groups of Y336 or TYN336 (Figure S5). As exemplified for wild type GS (Figure 5D), the binding of ATP to Y336 or TYN336 is further stabilized at this stage by hydrogen bonding with R45, W60, N61, and I206, as well as hydrophobic (with P208), cation-π (with R45), and chelating interactions (with Mg^{2+}). Together, these bonds lead to the overall drop in the PMFs of wild type GS and GS_{TYN} and the small local minima in phase II, from which ATP escapes to reach phase III. Finally, in phase III of ATP binding ($d \leq 6$ Å), ATP attains a bound state with a global minimum at $d \approx 3.7$ Å for all three GS variants (Figure 5A). The location of this minimum is in excellent agreement with the location of the peak of the most frequently sampled distance in unbiased MD simulations (Figure 5A). To conclude, the PMF computations indicate that Y336 nitration influences the thermodynamics of ATP binding to GS, but not the kinetics of this binding.

Nitrated Y336 Predominantly Exists in the Deprotonated TYD Form. The pK_a value of the phenolic hydroxyl group belonging to free 3′-nitrotyrosine is 3 log units lower than that of tyrosine[19] (Figure 1B). Local protein environments can further influence the pK_a of ionizable residues.[42] To probe for such an influence, we computed the pK_a shift of TYN336 relative to free 3′-nitrotyrosine according to eq 6 (see Supporting Information for details). The relevant $\Delta\Delta G$ values were computed by evaluating the thermodynamic cycle depicted in Figure 6A employing TI.[43,44] These calculations were done by the use of acetyl-capped and *N*-methyl-capped TYN and TYD as model systems for (free) 3′-nitro tyrosine. The transformations from (free) TYN into TYD, and TYN336 into TYD336, yields $\Delta\Delta G = -2.72$ kcal mol^{-1} (SEM < 0.01 kcal mol^{-1}), which in turn suggests a marked decrease in the pK_a of TYN336 of approximately 2 log units to a pK_a of 5.3 (Figure 6A). Hence, at a physiological pH of 7.4, greater than 99% of all nitrated Y336 are in the TYD336 state, such that only the negatively charged variant is relevant under physiological conditions. This also applies with respect to the experimental conditions previously chosen.[20−24] The observations that nitration of Y336 decreases the pK_a of its phenolic hydroxyl group and that binding of ATP to GS_{TYD} is weakened (see above) are consistent with the finding that GS activity is inhibited under physiological conditions.[20,21] One implication of these observations is that the inhibition of GS activity by Y336 nitration should be relieved by lowering the pH below the pK_a of the nitrated Y336. At pH 4, for example, 95% of the

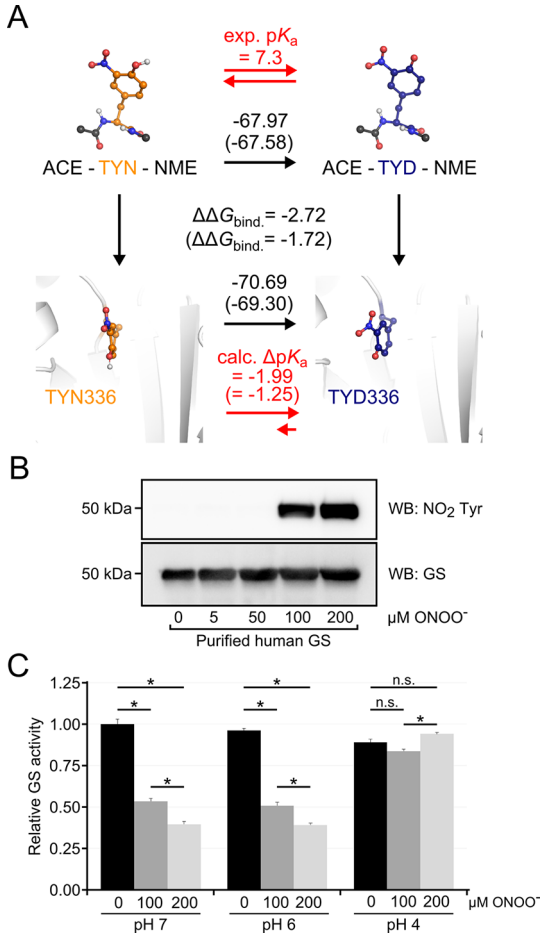

Figure 6. pH-sensitive inhibition of GS activity. (A) Thermodynamic cycle employed for studying the protonation state of nitrated Y336. The free energy differences ΔG were calculated by thermodynamic integration for transformations of TYN into TYD (top panel depicts the transformation for ACE-TYN/TYD-NME, the bottom panel for TYN336/TYD336 in the GS structure). If ΔG, $\Delta\Delta G$, and ΔpK_a are reported in parentheses, the endpoints $\lambda = 0.0$ and $\lambda = 1.0$ were not considered for integration. The difference in free energy $\Delta\Delta G$ was calculated according to eq 6 and the pK_a shift (calc. ΔpK_a) according to eq 5 (see Supporting Information and Materials and Methods for details). The experimentally determined pK_a (exp. pK_a) was measured for free 3-nitro tyrosine.[25] At physiological pH (~7.4), the TYD state in GS is preferred over the TYN state (schematically depicted by red arrows). (B) *In vitro* nitration of purified human GS. Purified human GS was exposed to vehicle (0 μM $ONOO^-$, control) or different concentrations of $ONOO^-$ (5, 50, 100, or 200 μM), and 3′-nitrotyrosine (top) and non-nitrated GS (bottom) were detected by Western Blot analysis. (C) pH dependence of $ONOO^-$-mediated inhibition of GS activity. Purified human GS was exposed to different concentrations of $ONOO^-$ (0, 100, or 200 μM), and aliquots were taken for measuring GS activity as described in the Supporting Information and Materials and Methods. GS activity in vehicle-treated control at pH 7.0 was set to 1, and activities measured under the other experimental conditions are given relative to it. ∗: Statistically significantly different ($p < 0.05$). n.s.: Not statistically significantly different.

https://dx.doi.org/10.1021/acs.jctc.0c00249
J. Chem. Theory Comput. 2020, 16, 4694−4705

nitrated Y336 should be in the protonated TYN336 state, for which our computations suggest an increased binding affinity to ATP.

Peroxynitrite-Induced Tyrosine Nitration of Human GS. In order to test the hypothesis that lowering pH would relieve inhibition of GS activity due to Y336 nitration, we first established that peroxynitrite ($ONOO^-$) causes the nitration of human GS. Thus, purified human GS was exposed to 0, 5, 50, 100, or 200 μM $ONOO^-$ and then analyzed for the content of nitrated and total GS by Western Blot. As shown in Figure 6B, $ONOO^-$ induces a concentration-dependent increase of GS NO_2–Tyr immunoreactivity that is particularly evident at higher $ONOO^-$ concentrations. $ONOO^-$, however, has no effect on anti-GS immunoreactivity at concentrations as high as 200 μM (Figure 6B). Thus, under our experimental conditions, exposure of human GS to $ONOO^-$ results in the nitration of this enzyme but not its degradation.

Effects of Peroxynitrite on Catalytic Activity of Human GS. Next, purified human GS was exposed to different concentrations of $ONOO^-$ (0, 100, and 200 μM), and catalytic activity of GS was measured in reaction mixtures adjusted to pH 7.0, 6.0, or 4.0 (see Supporting Information for details). As shown in Figure 6C, GS activity was significantly reduced in samples treated with 100 or 200 μM $ONOO^-$ as compared to vehicle-exposed controls (0 μM) at pH 7 and to a similar extent at pH 6. Lowering the pH of the reaction mixture to 4, however, restored GS activity in $ONOO^-$-exposed samples to control values. At pH 4, GS activity was significantly higher in samples exposed to 200 μM rather than 100 μM $ONOO^-$, presumably reflecting the greater extent of nitration depicted in Figure 6B. The activity of nitrated GS is restored by incubation at pH 4 and not pH 6 or 7.

DISCUSSION

The molecular mechanism of how Y336 nitration leads to inhibition of GS catalytic activity was unknown. Here, we show using unbiased MD simulations, as well as binding and configurational free energy computations that Y336 nitration hampers substrate (ATP) binding, but only in the deprotonated and negatively charged TYD336 state. By contrast, our calculations indicate an increased binding affinity of the protonated and neutral TYN336 state for ATP. pK_a computations of nitrated Y336 within GS predict a pK_a of approximately 5 such that under physiological pH conditions (pH $\approx$ 7.4) nitrated Y336 almost exclusively exists in the TYD336 state. *In vitro* experiments confirm these predictions, in that catalytic activity of tyrosine-nitrated GS is decreased at pH 7 and pH 6, but not at pH 4. Furthermore, at pH 4, GS activity was significantly higher in samples exposed to 200 μM compared to 100 μM $ONOO^-$. Together, these data reveal a unique pH-sensitive mechanism of GS inhibition due to the nitration of Y336.

Our computational results suggest that stacking interactions between Y336/TYN336/TYD336 and ATP (Figure 1A) are weakened in the TYD336 state, and this weakening is the most likely cause for the decreased affinity of nitrated GS for ATP. These results are based on five independent MD simulations performed for wild type GS, as well as GS_{TYN} and GS_{TYD} variants (for a detailed assessment of the computational procedures used, see Supporting Information.) Using the distance d and angle η between the phenyl ring of Y336/TYN33/TYD336 and the purine ring system of ATP to characterize respective stacking geometries, a predominately coplanar arrangement of both rings for wild type GS was revealed ($d \approx 3.8$ Å and $\eta \approx 8°$; Figure 2A–C). This coplanar arrangement is temporarily absent for GS_{TYN} and GS_{TYD} ($d \approx 5.5$ Å and $\eta \approx 40°$; $d \approx 7.7$ Å and $\eta \approx 132°$ Figure 2A-C). As *ab initio* calculations indicate strong interactions between tyrosine and adenine for distances less than 4 Å and plane angles approximately equal to 10°,[40] these structural assessments suggest that Y336 nitration weakens interactions with ATP, in particular, between TYD336 and ATP. These results mirror the analysis of atomic mobility of bound ATP (Figure 2D).

In line with the structural analyses, effective binding energy calculations for ATP binding to nitrated GS variants reveal disfavored ATP binding to GS_{TYD} relative to wild type GS (Figure 3). These calculations also revealed that ATP binding is favored to GS_{TYN} relative to wild type GS. These results were confirmed by TI computations (Figure 4). The quantitative differences between these independent methods are in the range of the chemical/computational accuracy of free energy calculations.[45−47] In contrast to MM-PBSA and TI calculations, PMF computations provide an energetic estimate for the full ATP binding process. We note that the difference in the PMF between the unbound and the completely bound state does not equate to an absolute binding free energy.[48] Yet, considering that the specified reaction coordinate is the same in all three investigated cases and that the sampled unbound state is very similar (Figure 5B), the differences in the PMFs relative to the unbound state can be interpreted as differences in the binding energetics among the three systems. Hence, the PMF computations also support the results from MM-PBSA and TI calculations.

For TYN336, a pK_a shift of approximately 2 log units was computed relative to (free) TYN in solution (Figure 6A). Such a magnitude of a pK_a shift is within the range of pK_a shifts reported before for titratable amino acids by experiments and computations.[49−51] The uncertainty in our free energy computation is in fair agreement with those reported in related studies.[52] Together with the above structural and energetic analyses of ATP binding to GS_{TYD} or GS_{TYN} versus wild type GS, the pK_a computations led to the prediction that nitrated GS is less active at physiological pH, where GS_{TYD} is almost exclusively present, whereas increased activity is expected at acidic pH, where GS_{TYN} is favored.

These findings are supported by our *in vitro* experiments showing a reduced catalytic activity of nitrated GS at pH 7 and 6, but not at pH 4 (Figure 6C). Importantly, within this pH-range, 3′-nitrotyrosine was reported to be chemically stable,[53] thereby ruling out that a chemical denitration accounts for the recovery of the catalytic activity. The data of the present study also corroborate previous findings showing that nitration of rat, sheep, or human GS inhibits their catalytic activity at physiological pH.[20,21,54,55] Notably, in line with the computational predictions that ATP binding to GS_{TYN} is more favorable (Figures 3A, 4, 5A), GS activity is significantly higher in samples exposed to 200 μM as compared to 100 μM $ONOO^-$ at pH 4.0. A plausible explanation for the increased stacking interactions between TYN336 and ATP is that the electron-withdrawing effect of the nitro group may reduce repulsive forces between the phenyl ring and the electron-rich purine ring system of ATP.[56] A similar effect has been reported for aldose reductase inhibitors bearing an *m*-nitrophenyl group.[57] By contrast, the additional negative charge on TYD336 increases the electron density in the phenolate ring, which

https://dx.doi.org/10.1021/acs.jctc.0c00249
J. Chem. Theory Comput. 2020, 16, 4694−4705

may increase repulsive forces with the electron-rich purine ring system of ATP and, hence, lead to weak stacking interactions.

Modifications other than Y336 nitration[20,22] may account for the loss of activity of human GS subjected to nitrooxidative stress. One such modification is the formation of a dityrosine linkage between Y185 and Y269, leading to the generation of high molecular GS aggregates.[58] However, we did not detect high molecular aggregates even after treatment of native GS with 200 μM $ONOO^-$ (Figure 6B). Mapping of Y185 and Y269 onto the crystal structure of human GS[2] reveals that neither residue makes a direct interaction with a GS substrate; instead, they are located on the protein surface (Figure S6). Hence, a direct influence of Y185 or Y269 nitration on the catalytic mechanism appears unlikely. While our computational results in connection with our experimental data strongly point to nitrated Y336 as the origin of the loss of activity of human GS subjected to nitrooxidative stress, we cannot fully exclude the possibility that this loss arises due to another or additional nitration or that (de)protonation of another residue leads to the experimental observations. As for the former, mass spectrometry experiments provided strong evidence that Y336 is the target for nitration, although Y161 was also discussed as a potential target.[20,22] As for the latter, a site-specific detection of protonation changes would be required, which is beyond the scope of the current study.

Recently, the molecular consequences of PTN on human manganese superoxide dismutase (MnSOD) were investigated by steered MD simulations.[59] Y34 nitration inhibits MnSOD[60] by hampering the passage of the superoxide radical anion in the channel leading to the active center.[59] The authors found a high energetic barrier on the way to the active site for both 3′-nitrotyrosine variants[59] that they attributed to steric effects.[61] By contrast, our computations indicate that Y336 nitration in GS impacts the *affinity* of the modified enzyme for ATP, rather than the binding *kinetics*, and it does so with opposite effects depending on the TYD336 or TYN336 state of the tyrosyl residue. This comparison thus suggests that the underlying effect of tyrosine nitration on enzyme activity depends on the type of substrate and/or topology of the binding site. As to the latter, while MnSOD's binding site resembles a binding channel that can be blocked by the insertion of a single nitro group,[19,59] the GS binding site is bifunnel shaped[17] with Y336 located at the top of the funnel (Figure S6). Thus, ATP, in particular, the negatively charged phosphate groups, might have enough room to escape the direct influence of nitrated Y336 during the binding process.

So far, tyrosine nitration is thought to have one of three effects on protein function: loss of function, a gain of function, or no change on protein function (for a comprehensive review, see ref 62). As to the latter, only two proteins have been reported to date (antichymotrypsin and transferrin).[62,63] Cytochrome c is a well-studied example for a gain of function, in which nitration triggers structural rearrangements yielding a protein conformation with increased catalytic activity.[62,64,65] Proteins that show a loss of function after tyrosine nitration form the largest group,[62] and so far, human GS is considered part of this group as well.[20,21,54,55] However, here, we provide the first evidence that indicates that the inhibitory effect of Y336 nitration is fully reversible depending on the pH of the protein environment. To our knowledge, these results suggest a novel mechanism for the regulation of protein function by PTN.

Pathological ammonia concentrations trigger oxidation processes, including the nitration of tyrosine, in rat and human brains, respectively.[7,20,21] GS nitration and the related deficiency in GS function are associated with a broad range of neurological diseases,[16,66,67] including Alzheimer's disease.[68,69] It has been hypothesized that human GS is sensitive to age-related oxidation.[69] The lack of GS activity due to nitration progressively leads to incomplete ammonia detoxification, which in turn promotes a vicious circle, where increases in ammonia[7,20,21] foster further oxidation and/or nitration of GS. Furthermore, the hyperammonemic conditions may lead to pH increases that may further reduce GS activity.

CONCLUSION

How Y336 nitration leads to inhibition of human GS catalytic activity was unknown. Combining computational chemistry methods with functional *in vitro* experiments, we found that Y336 nitration weakens interactions between human GS and the substrate ATP but only in its negatively charged TYD336 state. Furthermore, our computations suggest that only TYD336 is relevant under physiological conditions. By contrast, for the protonated and neutral TYN336 state, an increased binding affinity for ATP is predicted and supported by a significantly higher GS activity in samples exposed to 200 μM $ONOO^-$. These results indicate a novel, fully reversible, and pH-sensitive mechanism for the regulation of protein function by tyrosine nitration. We speculate that such an arrangement may keep enzymes in an inactive state in the cytosol but trigger their activation after translocation into an acidic compartment, such as lysosomes. Since the pK_a values of 3′-nitrotyrosine vary markedly, depending on their location within proteins, the effect of pH on the impact of tyrosine nitration on protein function will have to be considered in evaluating existing and future studies of this modification.[62]

ASSOCIATED CONTENT

Supporting Information

The Supporting Information is available free of charge at https://pubs.acs.org/doi/10.1021/acs.jctc.0c00249.

Figures S1−S11, Tables S1−S5, detailed Materials and Methods section, and section about assessment of computational procedures (PDF)

AUTHOR INFORMATION

Corresponding Authors

Dieter Häussinger − *Clinic for Gastroenterology, Hepatology, and Infectious Diseases, Heinrich Heine University Düsseldorf, Düsseldorf, Germany*; Phone: (+49) 211 81 16330; Email: haeussin@uni-duesseldorf.de; Fax: (+49) 211 81 18752

Holger Gohlke − *Institute for Pharmaceutical and Medicinal Chemistry, Heinrich Heine University Düsseldorf, Düsseldorf, Germany; John von Neumann Institute for Computing (NIC), Jülich Supercomputing Centre (JSC), and Institute of Biological Information Processing (IBI-7: Structural Biochemistry), Forschungszentrum Jülich GmbH, Jülich, Germany;* orcid.org/0000-0001-8613-1447; Phone: (+49) 211 81 13662; Email: gohlke@uni-duesseldorf.de, h.gohlke@fz-juelich.de; Fax: (+49) 211 81 13847

https://dx.doi.org/10.1021/acs.jctc.0c00249
J. Chem. Theory Comput. 2020, 16, 4694−4705

Authors

Benedikt Frieg − *Institute for Pharmaceutical and Medicinal Chemistry, Heinrich Heine University Düsseldorf, Düsseldorf, Germany; John von Neumann Institute for Computing (NIC), Jülich Supercomputing Centre (JSC), and Institute of Biological Information Processing (IBI-7: Structural Biochemistry), Forschungszentrum Jülich GmbH, Jülich, Germany*

Boris Görg − *Clinic for Gastroenterology, Hepatology, and Infectious Diseases, Heinrich Heine University Düsseldorf, Düsseldorf, Germany*

Natalia Qvartskhava − *Clinic for Gastroenterology, Hepatology, and Infectious Diseases, Heinrich Heine University Düsseldorf, Düsseldorf, Germany*

Thomas Jeitner − *Department of Biochemistry and Molecular Biology, New York Medical College, Valhalla, New York 10595, United States*

Nadine Homeyer − *Institute for Pharmaceutical and Medicinal Chemistry, Heinrich Heine University Düsseldorf, Düsseldorf, Germany*

Complete contact information is available at: https://pubs.acs.org/10.1021/acs.jctc.0c00249

Author Contributions

B.G., D.H., and H.G. conceived and designed the experiments. B.F., B.G., N.Q., N.H., and T.J. performed the experiments. B.F., B.G., N.H., D.H. and H.G. analyzed the data. B.F., B.G., T.J., N.H., D.H., and H.G. wrote the paper.

Funding

Financial support by Deutsche Forschungsgemeinschaft (DFG) for funds (INST 208/704-1 FUGG) to purchase the hybrid computer cluster used in this study is gratefully acknowledged by H.G. This work was supported by the Deutsche Forschungsgemeinschaft through the Collaborative Research Center SFB 974 ("Communication and Systems Relevance during Liver Damage and Regeneration", Düsseldorf, 190586431).).

Notes

The authors declare no competing financial interest.

■ ACKNOWLEDGMENTS

B.F. and H.G. are grateful to the Jülich Supercomputing Centre at the Forschungszentrum Jülich for computing time on the supercomputer JURECA and JUWELS (NIC project ID: HKF7) and to the "Zentrum für Informations- und Medientechnologie" (ZIM) at the Heinrich Heine University Düsseldorf for providing computational support.

■ ABBREVIATIONS

GS = Glutamine synthetase
MD = Molecular dynamics
MM-PBSA = Molecular mechanics Poisson−Boltzmann surface area
PMF = Potential of mean force
SEM = Standard error of the mean
TI = Thermodynamic integration
US = Umbrella sampling
WHAM = Weighted histogram analysis method

■ REFERENCES

(1) Meister, A. Glutamine synthetase from mammalian tissues. *Methods Enzymol.* **1985**, *113*, 185−199.

(2) Krajewski, W. W.; Collins, R.; Holmberg-Schiavone, L.; Jones, T. A.; Karlberg, T.; Mowbray, S. L. Crystal structures of mammalian glutamine synthetases illustrate substrate-induced conformational changes and provide opportunities for drug and herbicide design. *J. Mol. Biol.* **2008**, *375* (1), 217−28.

(3) Martinez-Hernandez, A.; Bell, K. P.; Norenberg, M. D. Glutamine synthetase: glial localization in brain. *Science* **1977**, *195* (4284), 1356−8.

(4) Petroff, O. A. C.; Errante, L. D.; Rothman, D. L.; Kim, J. H.; Spencer, D. D. Glutamate-glutamine cycling in the epileptic human hippocampus. *Epilepsia* **2002**, *43* (7), 703−710.

(5) Häussinger, D. Hepatocyte heterogeneity in glutamine and ammonia metabolism and the role of an intercellular glutamine cycle during ureogenesis in perfused-rat-liver. *Eur. J. Biochem.* **1983**, *133* (2), 269−275.

(6) Häussinger, D.; Sies, H.; Gerok, W. Functional hepatocyte heterogeneity in ammonia metabolism. *J. Hepatol.* **1985**, *1* (1), 3−14.

(7) Qvartskhava, N.; Lang, P. A.; Görg, B.; Pozdeev, V. I.; Ortiz, M. P.; Lang, K. S.; Bidmon, H. J.; Lang, E.; Leibrock, C. B.; Herebian, D.; Bode, J. G.; Lang, F.; Häussinger, D. Hyperammonemia in gene-targeted mice lacking functional hepatic glutamine synthetase. *Proc. Natl. Acad. Sci. U. S. A.* **2015**, *112* (17), 5521−5526.

(8) Häussinger, D. Nitrogen metabolism in liver: structural and functional organization and physiological relevance. *Biochem. J.* **1990**, *267* (2), 281−290.

(9) Häussinger, D. Hepatic glutamine transport and metabolism. *Adv. Enzymol. Relat. Areas. Mol. Biol.* **2006**, *72*, 43−86.

(10) Gunnersen, D.; Haley, B. Detection of glutamine synthetase in the cerebrospinal-fluid of Alzheimer diseased patients - a potential diagnostic biochemical marker. *Proc. Natl. Acad. Sci. U. S. A.* **1992**, *89* (24), 11949−11953.

(11) Tumani, H.; Shen, G.; Peter, J. B.; Bruck, W. Glutamine synthetase in cerebrospinal fluid, serum, and brain: a diagnostic marker for Alzheimer disease? *Arch. Neurol.* **1999**, *56* (10), 1241−6.

(12) Brusilow, S. W.; Koehler, R. C.; Traystman, R. J.; Cooper, A. J. L. Astrocyte glutamine synthetase: importance in hyperammonemic syndromes and potential target for therapy. *Neurotherapeutics* **2010**, *7* (4), 452−470.

(13) Häussinger, D.; Laubenberger, J.; Vom Dahl, S.; Ernst, T.; Bayer, S.; Langer, M.; Gerok, W.; Hennig, J. Proton magnetic-resonance spectroscopy studies on human brain myo-Iinositol in hypo-osmolarity and hepatic-encephalopathy. *Gastroenterology* **1994**, *107* (5), 1475−1480.

(14) Häussinger, D.; Kircheis, G.; Fischer, R.; Schliess, F.; vom Dahl, S. Hepatic encephalopathy in chronic liver disease: a clinical manifestation of astrocyte swelling and low-grade cerebral edema? *J. Hepatol.* **2000**, *32* (6), 1035−1038.

(15) Eid, T.; Behar, K.; Dhaher, R.; Bumanglag, A. V.; Lee, T. S. W. Roles of glutamine synthetase inhibition in epilepsy. *Neurochem. Res.* **2012**, *37* (11), 2339−2350.

(16) Eid, T.; Thomas, M. J.; Spencer, D. D.; Runden-Pran, E.; Lai, J. C. K.; Malthankar, G. V.; Kim, J. H.; Danbolt, N. C.; Ottersen, O. P.; de Lanerolle, N. C. Loss of glutamine synthetase in the human epileptogenic hippocampus: possible mechanism for raised extracellular glutamate in mesial temporal lobe epilepsy. *Lancet* **2004**, *363* (9402), 28−37.

(17) Eisenberg, D.; Gill, H. S.; Pfluegl, G. M.; Rotstein, S. H. Structure-function relationships of glutamine synthetases. *Biochim. Biophys. Acta, Protein Struct. Mol. Enzymol.* **2000**, *1477* (1−2), 122−45.

(18) Frieg, B.; Görg, B.; Homeyer, N.; Keitel, V.; Häussinger, D.; Gohlke, H. Molecular mechanisms of glutamine synthetase mutations that lead to clinically relevant pathologies. *PLoS Comput. Biol.* **2016**, *12* (2), No. e1004693.

(19) Radi, R. Protein tyrosine nitration: biochemical mechanisms and structural basis of functional effects. *Acc. Chem. Res.* **2013**, *46* (2), 550−559.

(20) Görg, B.; Wettstein, M.; Metzger, S.; Schliess, F.; Häussinger, D. Lipopolysaccharide-induced tyrosine nitration and inactivation of

hepatic glutamine synthetase in the rat. *Hepatology* **2005**, *41* (5), 1065−1073.
(21) Görg, B.; Qvartskhava, N.; Voss, P.; Grune, T.; Häussinger, D.; Schliess, F. Reversible inhibition of mammalian glutamine synthetase by tyrosine nitration. *FEBS Lett.* **2007**, *581* (1), 84−90.
(22) Görg, B.; Wettstein, M.; Metzger, S.; Schliess, F.; Häussinger, D. LPS-induced tyrosine nitration of hepatic glutamine synthetase. *Hepatology* **2005**, *42* (2), 499−499.
(23) Görg, B.; Bidmon, H. J.; Keitel, V.; Foster, N.; Goerlich, R.; Schliess, F.; Häussinger, D. Inflammatory cytokines induce protein tyrosine nitration in rat astrocytes. *Arch. Biochem. Biophys.* **2006**, *449* (1−2), 104−114.
(24) Görg, B.; Foster, N.; Reinehr, R.; Bidmon, H. J.; Hongen, A.; Häussinger, D.; Schliess, F. Benzodiazepine-induced protein tyrosine nitration in rat astrocytes. *Hepatology* **2003**, *37* (2), 334−342.
(25) Radi, R. Nitric oxide, oxidants, and protein tyrosine nitration. *Proc. Natl. Acad. Sci. U. S. A.* **2004**, *101* (12), 4003−8.
(26) Souza, J. M.; Peluffo, G.; Radi, R. Protein tyrosine nitration - functional alteration or just a biomarker? *Free Radical Biol. Med.* **2008**, *45* (4), 357−366.
(27) Joo, H. K.; Park, Y. W.; Jang, Y. Y.; Lee, J. Y. Structural analysis of glutamine synthetase from Helicobacter pylori. *Sci. Rep.* **2018**, *8*, na DOI: 10.1038/s41598-018-30191-5.
(28) Salomon-Ferrer, R.; Götz, A. W.; Poole, D.; Le Grand, S.; Walker, R. C. Routine microsecond molecular dynamics simulations with Amber on GPUs. 2. Explicit solvent particle mesh Ewald. *J. Chem. Theory Comput.* **2013**, *9* (9), 3878−3888.
(29) Bhati, A. P.; Wan, S. Z.; Wright, D. W.; Coveney, P. V. Rapid, accurate, precise, and reliable relative free energy prediction using ensemble based thermodynamic integration. *J. Chem. Theory Comput.* **2017**, *13* (1), 210−222.
(30) Loccisano, A. E.; Acevedo, O.; DeChancie, J.; Schulze, B. G.; Evanseck, J. D. Enhanced sampling by multiple molecular dynamics trajectories: carbonmonoxy myoglobin 10 mu s A0 -> A(1−3) transition from ten 400 ps simulations. *J. Mol. Graphics Modell.* **2004**, *22* (5), 369−376.
(31) Likic, V. A.; Gooley, P. R.; Speed, T. P.; Strehler, E. E. A statistical approach to the interpretation of molecular dynamics simulations of calmodulin equilibrium dynamics. *Protein Sci.* **2005**, *14* (12), 2955−2963.
(32) Steinbrecher, T.; Joung, I.; Case, D. A. Soft-core potentials in thermodynamic integration: comparing one- and two-step transformations. *J. Comput. Chem.* **2011**, *32* (15), 3253−63.
(33) Michel, J.; Essex, J. W. Prediction of protein-ligand binding affinity by free energy simulations: assumptions, pitfalls and expectations. *J. Comput.-Aided Mol. Des.* **2010**, *24* (8), 639−658.
(34) Kottalam, J.; Case, D. A. Dynamics of ligand escape from the heme pocket of myoglobin. *J. Am. Chem. Soc.* **1988**, *110* (23), 7690−7697.
(35) Kumar, S.; Bouzida, D.; Swendsen, R. H.; Kollman, P. A.; Rosenberg, J. M. The weighted histogram analysis method for free-energy calculations on biomolecules. 1. The method. *J. Comput. Chem.* **1992**, *13* (8), 1011−1021.
(36) Simonson, T.; Carlsson, J.; Case, D. A. Proton binding to proteins: pK(a) calculations with explicit and implicit solvent models. *J. Am. Chem. Soc.* **2004**, *126* (13), 4167−4180.
(37) Listrom, C. D.; Morizono, H.; Rajagopal, B. S.; McCann, M. T.; Tuchman, M.; Allewell, N. M. Expression, purification, and characterization of recombinant human glutamine synthetase. *Biochem. J.* **1997**, *328*, 159−163.
(38) Jeitner, T. M.; Cooper, A. J. L. Inhibition of human glutamine synthetase by L-methionine-S, R-sulfoximine-relevance to the treatment of neurological diseases. *Metab. Brain Dis.* **2014**, *29* (4), 983−989.
(39) Kingdon, H. S.; Hubbard, J. S.; Stadtman, E. R. Regulation of glutamine synthetase. XI. The nature and implications of a lag phase in the Escherichia coli glutamine synthetase reaction. *Biochemistry* **1968**, *7* (6), 2136−2142.
(40) Copeland, K. L.; Pellock, S. J.; Cox, J. R.; Cafiero, M. L.; Tschumper, G. S. Examination of Tyrosine/Adenine Stacking Interactions in Protein Complexes. *J. Phys. Chem. B* **2013**, *117* (45), 14001−14008.
(41) Ludemann, S. K.; Lounnas, V.; Wade, R. C. How do substrates enter and products exit the buried active site of cytochrome P450cam? 1. Random expulsion molecular dynamics investigation of ligand access channels and mechanisms. *J. Mol. Biol.* **2000**, *303* (5), 797−811.
(42) Li, H.; Robertson, A. D.; Jensen, J. H. Very fast empirical prediction and rationalization of protein pKa values. *Proteins: Struct., Funct., Genet.* **2005**, *61* (4), 704−21.
(43) Homeyer, N.; Stoll, F.; Hillisch, A.; Gohlke, H. Binding free energy calculations for lead optimization: Assessment of their accuracy in an industrial drug design context. *J. Chem. Theory Comput.* **2014**, *10*, 3331−3344.
(44) Steinbrecher, T.; Case, D. A.; Labahn, A. A multistep approach to structure-based drug design: studying ligand binding at the human neutrophil elastase. *J. Med. Chem.* **2006**, *49* (6), 1837−1844.
(45) Cournia, Z.; Allen, B.; Sherman, W. Relative binding free energy calculations in drug discovery: recent advances and practical considerations. *J. Chem. Inf. Model.* **2017**, *57* (12), 2911−2937.
(46) Wang, L.; Wu, Y. J.; Deng, Y. Q.; Kim, B.; Pierce, L.; Krilov, G.; Lupyan, D.; Robinson, S.; Dahlgren, M. K.; Greenwood, J.; Romero, D. L.; Masse, C.; Knight, J. L.; Steinbrecher, T.; Beuming, T.; Damm, W.; Harder, E.; Sherman, W.; Brewer, M.; Wester, R.; Murcko, M.; Frye, L.; Farid, R.; Lin, T.; Mobley, D. L.; Jorgensen, W. L.; Berne, B. J.; Friesner, R. A.; Abel, R. Accurate and reliable prediction of relative ligand binding potency in prospective drug discovery by way of a modern free-energy calculation protocol and force field. *J. Am. Chem. Soc.* **2015**, *137* (7), 2695−2703.
(47) Steinbrecher, T.; Abel, R.; Clark, A.; Friesner, R. Free energy perturbation calculations of the thermodynamics of protein side-chain mutations. *J. Mol. Biol.* **2017**, *429* (7), 923−929.
(48) Doudou, S.; Burton, N. A.; Henchman, R. H. Standard free energy of binding from a one-dimensional potential of mean force. *J. Chem. Theory Comput.* **2009**, *5* (4), 909−918.
(49) Onufriev, A. V.; Alexov, E. Protonation and pK changes in protein-ligand binding. *Q. Rev. Biophys.* **2013**, *46* (2), 181−209.
(50) Ranganathan, A.; Dror, R. O.; Carlsson, J. Insights into the role of Asp79(2.50) in beta(2) adrenergic receptor activation from molecular dynamics simulations. *Biochemistry* **2014**, *53* (46), 7283−7296.
(51) Stanton, C. L.; Houk, K. N. Benchmarking pKa prediction methods for residues in proteins. *J. Chem. Theory Comput.* **2008**, *4* (6), 951−66.
(52) Giese, T. J.; York, D. M. A GPU-accelerated parameter interpolation thermodynamic integration free energy method. *J. Chem. Theory Comput.* **2018**, *14* (3), 1564−1582.
(53) Liu, M. C.; Yasuda, S.; Idell, S. Sulfation of nitrotyrosine: Biochemistry and functional implications. *IUBMB Life* **2007**, *59* (10), 622−627.
(54) Görg, B.; Qvartskhava, N.; Bidmon, H. J.; Palomero-Gallagher, N.; Kircheis, G.; Zilles, K.; Häussinger, D. Oxidative stress markers in the brain of patients with cirrhosis and hepatic encephalopathy. *Hepatology* **2010**, *52* (1), 256−265.
(55) Schliess, F.; Görg, B.; Fischer, R.; Desjardins, P.; Bidmon, H. J.; Herrmann, A.; Butterworth, R. F.; Zilles, K.; Häussinger, D. Ammonia induces MK-801-sensitive nitration and phosphorylation of protein tyrosine residues in rat astrocytes. *FASEB J.* **2002**, *16* (3), 739−741.
(56) Martinez, C. R.; Iverson, B. L. Rethinking the term ″pi-stacking. *Chem. Sci.* **2012**, *3* (7), 2191−2201.
(57) Steuber, H.; Heine, A.; Klebe, G. Structural and thermodynamic study on aldose reductase: Nitro-substituted inhibitors with strong enthalpic binding contribution. *J. Mol. Biol.* **2007**, *368* (3), 618−638.
(58) Bartesaghi, S.; Campolo, N.; Issoglio, F.; Zeida, A.; Grune, T.; Estrín, D.; Radi, R. Oxidative inactivation of human glutamine

synthetase: biochemical and computational studies. *Free Radical Biol. Med.* **2016**, *100*, S19.
(59) Moreno, D. M.; Marti, M. A.; De Biase, P. M.; Estrin, D. A.; Demicheli, V.; Radi, R.; Boechi, L. Exploring the molecular basis of human manganese superoxide dismutase inactivation mediated by tyrosine 34 nitration. *Arch. Biochem. Biophys.* **2011**, *507* (2), 304−9.
(60) Yamakura, F.; Taka, H.; Fujimura, T.; Murayama, K. Inactivation of human manganese-superoxide dismutase by peroxynitrite is caused by exclusive nitration of tyrosine 34 to 3-nitrotyrosine. *J. Biol. Chem.* **1998**, *273* (23), 14085−14089.
(61) Quint, P.; Reutzel, R.; Mikulski, R.; McKenna, R.; Silverman, D. N. Crystal structure of nitrated human manganese superoxide dismutase: Mechanism of inactivation. *Free Radical Biol. Med.* **2006**, *40* (3), 453−458.
(62) Ferrer-Sueta, G.; Campolo, N.; Trujillo, M.; Bartesaghi, S.; Carballal, S.; Romero, N.; Alvarez, B.; Radi, R. Biochemistry of peroxynitrite and protein tyrosine nitration. *Chem. Rev.* **2018**, *118* (3), 1338−1408.
(63) Gole, M. D.; Souza, J. M.; Choi, I.; Hertkorn, C.; Malcolm, S.; Foust, R. F.; Finkel, B.; Lanken, P. N.; Ischiropoulos, H. Plasma proteins modified by tyrosine nitration in acute respiratory distress syndrome. *Am. J. Physiol. Lung Cell. Mol. Physiol.* **2000**, *278* (5), L961−L967.
(64) Batthyany, C.; Souza, J. M.; Duran, R.; Cassina, A.; Cervenansky, C.; Radi, R. Time course and site(s) of cytochrome c tyrosine nitration by peroxynitrite. *Biochemistry* **2005**, *44* (22), 8038−8046.
(65) Cassina, A. M.; Hodara, R.; Souza, J. M.; Thomson, L.; Castro, L.; Ischiropoulos, H.; Freeman, B. A.; Radi, R. Cytochrome c nitration by peroxynitrite. *J. Biol. Chem.* **2000**, *275* (28), 21409−21415.
(66) Spodenkiewicz, M.; Diez-Fernandez, C.; Rufenacht, V.; Gemperle-Britschgi, C.; Häberle, J. Minireview on glutamine synthetase deficiency, an ultra-rare inborn error of amino acid biosynthesis. *Biology (Basel, Switz.)* **2016**, *5* (4), 40.
(67) Leprince, G.; Delaere, P.; Fages, C.; Lefrancois, T.; Touret, M.; Salanon, M.; Tardy, M. Glutamine synthetase (GS) expression is reduced in senile dementia of the Alzheimer-type. *Neurochem. Res.* **1995**, *20* (7), 859−862.
(68) Robinson, S. R. Neuronal expression of glutamine synthetase in Alzheimer's disease indicates a profound impairment of metabolic interactions with astrocytes. *Neurochem. Int.* **2000**, *36* (4−5), 471−482.
(69) Smith, C. D.; Carney, J. M.; Starkereed, P. E.; Oliver, C. N.; Stadtman, E. R.; Floyd, R. A.; Markesbery, W. R. Excess brain protein oxidation and enzyme dysfunction in normal aging and in Alzheimer disease. *Proc. Natl. Acad. Sci. U. S. A.* **1991**, *88* (23), 10540−10543.

https://dx.doi.org/10.1021/acs.jctc.0c00249
J. Chem. Theory Comput. 2020, 16, 4694−4705